Investigating the Relationship Between Chemical Abundance Ratios and Ages in Red Giant Stars

Arthur Alencastro Puls

Research School of Astronomy and Astrophysics
Australian National University

Supervisory Panel:

Dr. David Yong
Dr. Luca Casagrande
Prof. Martin Asplund
Prof. Jorge Melendez (IAG-USP)

July 2019

Abstract

Stellar ages are, among other parameters, crucial to understand the history of formation and evolution of the Milky Way. In this context, a relationship mapping ages to chemistry has been sought. Recent developments have found significant correlations between ages and some chemical abundance ratios. However, these correlations have not been studied in depth in some regions of the Hertzsprung-Russell diagram. Here, I propose to investigate in detail the existence of a relationship between abundance ratios and ages – chemical clocks – in the Red Giant Branch, known to be plagued by an observational age-metallicity degeneracy, and in the red clump. I will rely on spectroscopic analysis – differential and classical – to infer the abundance ratios. For age estimation, information from asteroseismology will be used for field stars. I intend to divide the work in three parts. One is an ongoing analysis of chemically unusual stars that I intend to put into the context of chemical clocks. The other two are analyses of chemical clocks in both field and open cluster stars. The open cluster analysis will work as a control group to check if the results are homogeneous. Here, I intend to assemble an empirical grid for age inference in red giants, if the chemical clocks are confirmed, as well as developing skills in a second field of study besides spectroscopy – asteroseismology.

1 Introduction

The formation and evolution of galaxies is one of the big open questions in contemporary Astrophysics (Freeman & Bland-Hawthorn, 2002). In this context, the study of the Milky Way (hereafter, the Galaxy), provides unique and valuable information. It is the only galaxy where detailed information may be gathered using, for instance, all stages of stellar evolution (Bland-Hawthorn & Gerhard, 2016).

Stellar kinematics, chemistry and ages are crucial parameters to understand the formation and evolution of the Galaxy and calibrate stellar evolution models. While the former two parameters benefit from huge amounts of information being collected by ongoing surveys such as, e.g., Gaia (Gaia Collaboration et al., 2016), APOGEE (Majewski et al., 2017), GALAH (De Silva et al., 2015), Gaia-ESO (Gilmore et al., 2012) or SkyMapper (Wolf et al., 2018), the third parameter, stellar ages, has been lagging behind the other two in terms of amount of information available.

Stellar age is not an observable quantity, even for the Sun, whose age determination can reach less-than-Myr precision if measurements of meteoritic samples in laboratory are considered (Connelly et al., 2012). Ages of field stars and clusters have been inferred using several approaches (Soderblom, 2010). Two of them are isochrone fitting/placement and cosmochronometry. Isochrone fitting works by comparing stellar models of fixed age and metallicity (an isochrone) with stars in a colour-magnitude diagram (CMD), the observational counterpart of the Hertzsprung–Russell diagram (HRD), while isochrone placement is the approach where a single star is 'placed' in a grid of stellar models. The fitting techinique has relative success in the determination of ages of stellar clusters, with uncertainties of the order of 1 Gyr for older (11-13 Gyr, i.e., an uncertainty of $\sim$ 10 %) objects such as globular clusters (e.g., Dotter et al., 2011), allowed by the statistics provided by a simple population composed of hundreds or thousands of stars.

However, as stressed by Soderblom, the efficiency of isochrone placement is plagued by several complications. For instance, there is an age-metallicity degeneracy in certain regions of the HR diagram (see, e.g., Howes et al., 2019) and the shape of isochrone tracks is highly nonlinear. In the case of stellar clusters the degeneracy is lifted in certain regions of the HRD (e.g., main-sequence turnoff (MSTO)), allowing isochrone fitting – but in a HRD of field stars containing several different stellar populations the isochrone placement technique is usually impracticable in degenerate regions. Therefore, isochrone placement has limitations for estimating ages of field stars, and it does not work well for regions of the HR diagram such as the Red Giant Branch (RGB, see Fig. 1), where the age-metallicity degeneracy is stronger.

Cosmochronometry works as an independent check for chemical evolution models, because it is independent of the later and based on well-known

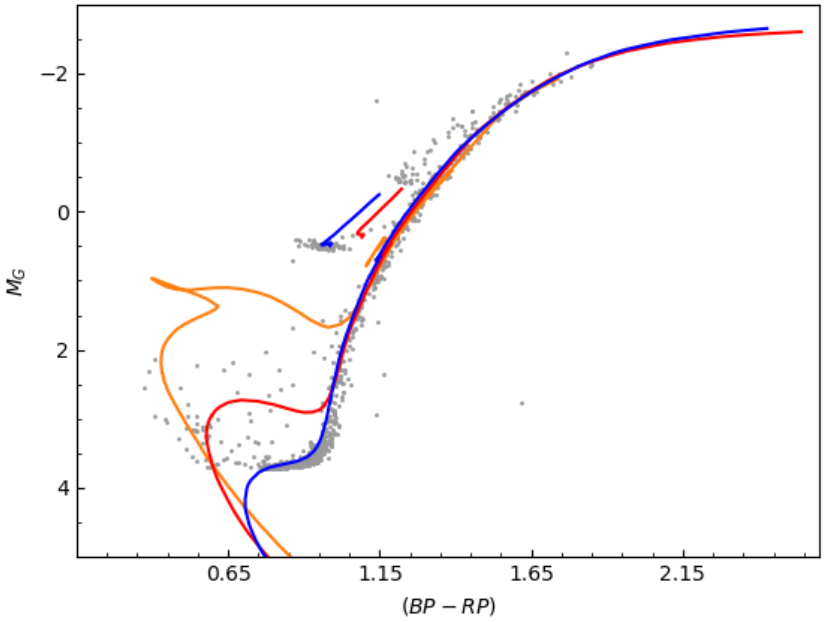

Figure 1: Colour-magnitude diagram, the observational counterpart of the HRD. Three PARSEC isochrones (Marigo et al., 2017) illustrate the age-metallicity degeneracy in the RGB: 1.5 Gyr–Z=0.0152 (orange), 4.5 Gyr–Z=0.0070 (red), 13 Gyr–Z=0.0040 (blue). Stars from the GC NGC 104, selected from Gaia DR2 proper motions (Gaia Collaboration et al., 2018), are shown for guidance (no isochrone fitting attempted). Distance modulus and extinction for NGC 104 calculated using data from the Harris (1996, 2010) catalog and calibrations from Cardelli et al. (1989) and O'Donnell (1994) available in the PARSEC output form.

physics (see Sneden et al., 2008, for a brief review within the context of neutron-capture nucleosynthesis and also Soderblom (2010) for a broader overview). Proposed by Butcher (1987), it works by measuring abundance ratios of long-lived radioactive isotopes to stable r-process elements. The rationale is the same employed in radiocarbon dating: the radioactive isotope will decay through the years, affecting the radioactive-to-stable ratio. It is an useful method for dating individual stars. However, this technique has some limitations. The spectral line used to estimate the abundance of (radioactive) Th is located in a crowded region of the electromagnetic spectrum, i.e., is subject to strong blends in metal-rich stars. Also, it needs a comparison (stable) element produced exclusively by the r-process. Eu is thought to be a near-pure r-process element through studies in the solar neighbourhood

(Simmerer et al., 2004) and has been used in more recent cosmochronometric determinations. However, the method assumes a stable r-process pattern, and any deviations from it may introduce bias in cosmochronometric ages. Finally, cosmochronometry is not totally model-independent, as it is relies on r-process modelling, as discussed, and nuclear physics constraints. Also, it assumes that the timescale between generations of stars is negligible – this might not be the rule.

This scenario where stellar ages estimations have low precision or are relatively well determined for only a few targets in the RGB has begun to change with more sophisticated multiparametric methods employing data from several large surveys (e.g., Queiroz et al., 2018) and space-based missions like CoRoT (Baglin et al., 2006), Kepler (Borucki et al., 2008) and K2 (Howell et al., 2014). While these observatories have been designed primarily to the search of exoplanets, the high-precision photometry delivered – with precision of the order of parts per million – allows the study of low-amplitude variability of their targets. Through the study of the stellar oscillations which generate this photometric variation – asteroseismology – we can derive properties such as mass, radius and mean density with precision of few percent (Chaplin & Miglio, 2013). Because the main-sequence lifetime is proportional to the initial mass of the star and the red giant lifetime is comparatively small, the mass of red giants is a good proxy for age. The basic concepts of asteroseismology will be further discussed in Section 2.2.

1.1 Motivation

Historically, a general age-metallicity relation (AMR) has been sought (e.g., Twarog, 1980; Edvardsson et al., 1993), under the assumption that the overall metallicity Z evolves with time as $\dot{Z} > 0$. Usually, [Fe/H][1] has been used as an observational proxy for Z, but it presents no clear trend with age and an intrinsic scatter even when controlled for selection effects (Feltzing et al., 2001). The lack of an observable AMR has been confirmed by measurements in wide binary systems with ages inferred from the evolutionary state of their white dwarf component, at least for ages below 7 Gyr (Rebassa-Mansergas et al., 2016). A more recent study from Silva Aguirre et al. (2018) found no evident AMR or age-[α/Fe] correlation in red giants from the APOKASC sample (Pinsonneault et al., 2014). However, an age-[α/Fe] relation has been found by other studies, being quite steep in the thick disc (e.g., Haywood et al., 2013).

The usage of [Fe/H] as observational metallicity is motivated by the large number of unblended Fe lines available in the spectra of late-type stars, but

[1]The square bracket notation represents the logarithmic ratio with respect to the ratio observed in the Sun. That is, [A/B] = log N_A/N_B - log $N_{A,\odot}/N_{B,\odot}$, where N_i is the column density of element i.

it is somewhat problematic. The Fe abundance in the solar photosphere is one order of magnitude smaller than that of O, the most abundant metal (Asplund et al., 2009). Also, the Fe/Z ratio is not constant in a star-to-star basis, being lower in α-enhanced and Carbon stars. Another example is the AMR in Galactic globular clusters (GGC): while the comparison between [Fe/H] and age shows a bifurcation that might be an indicative of accretion of some GGC, the older (> 9 Gyr) group extend on the full GGC [Fe/H] range, from [Fe/H] $\sim$ -2 to [Fe/H] $\sim$ 0 (Dotter et al., 2011; Leaman et al., 2013). The relationship between [Fe/H] and [α/Fe] is an useful tool to trace chemical evolution parameters such as the initial mass function and star formation rate, because it is able to trace the onset of Type Ia Supernovae (SNe), which produce much more Fe than α-elements, decreasing the [α/Fe], while Type II SNe yields a constant [α/Fe] ratio (e.g., Tinsley, 1979; Matteucci & Brocato, 1990; McWilliam, 1997, 2016). While important for chemical evolution diagnostics, the Fe content of the stars does not seem to be a reliable *direct* chemical clock.

Nissen (2015, 2016), using high quality spectra from solar twins to perform a differential analysis, found correlations between ages and several abundance ratios. Of those, [Y/Mg] is quite sensitive, decreasing by $\approx$ 0.04 dex/Gyr. Subsequent studies have extended the analysis for several other elements while Tucci Maia et al. (2016) have confirmed the [Y/Mg] clock with high statistical significance for solar twins. Further, it has been shown that the [Y/Al] ratio is a good chemical clock as well, at least for solar twins (Spina et al., 2016). Y, a predominantly s-process element, is therefore mainly produced in the Asymptotic Giant Branch (AGB) phase of low and intermediate mass[2] stars (Karakas & Lattanzio, 2014) while the main site for Mg are Type II SNe (Woosley & Weaver, 1995; Woosley et al., 2002; Kobayashi et al., 2006), the final stage of massive stars and, hence, characterized by a shorter timescale. The Y production peaks at 3 $M_{\odot}$ for solar metallicity (Cristallo et al., 2015; Karakas & Lugaro, 2016) while the Mg enrichment is slowed down in the longer timescales characteristic of the objects going through the AGB. Thus, as discussed by Feltzing et al. (2017), the sensitivity of [Y/Mg] to stellar age is a 'natural consequence' of Galactic chemical evolution. After a re-analysis of the large dwarf sample from Bensby et al. (2014) spanning a wide range of [Fe/H], Feltzing et al. (2017) showed that further measurements of the [Y/Mg] clock must control for [Fe/H], otherwise the resulting scatter would make the [Y/Mg] clock undetectable. This control occurred naturally in the aforementioned works from Nissen (2015, 2016), Tucci Maia et al. (2016) and Spina et al. (2016), because only solar twins (i.e., -0.15 < [Fe/H] < 0.15) were analysed.

While recent studies are increasing the dataset on chemical clocks for

[2]Here, 'low' mass stars are the ones that start the core He-burning phase with the He-flash.

dwarfs and MSTO stars (Delgado Mena et al., 2019; Titarenko et al., 2019), to my knowledge there is only one work on high precision chemical clocks in evolved stars published to date (Slumstrup et al., 2017). Their study measured the [Y/Mg] clock in a sample of 6 core He-burning stars from 4 solar metallicity open clusters. Also, works such as those from Martig et al. (2016) and Feuillet et al. (2018) present evidence for the relation between age and abundances of C and N in evolved stars, which is predicted by stellar evolution models. From this starting point, I propose a broad study about chemical clocks in red giants in different regions of the HRD, both in the RGB and core He-burning stages and from different metallicity regimes. The main questions to be addressed are 'What are the best chemical clocks for evolved stars? Do the age-[Y/Mg] and age-[Y/Al] relations found for solar twins hold in other stages of stellar evolution? If affirmative, do they have a similar slope for several evolutionary stages? Are there tight chemical clocks involving other s-process elements such as Ba – e.g., [Ba/Mg]?'. This proposal requires state-of-the-art data and methods. These methods will be discussed in the next Section.

2 Methods

In this section I will give an overview on the methods to be employed during my PhD. The main areas of interest here are asteroseismology and chemical analysis of stellar atmospheres through high resolution spectroscopy.

2.1 Chemical analysis

To study the [Y/Mg] and other potential chemical clocks we need to estimate the detailed surface chemical composition of the stars under scrutiny. This information in encoded in their electromagnetic spectra, shaped by the interactions occurring in their atmospheres. Each spectral line corresponds to an atomic or molecular transition[3] – if all other parameters that control the strength and shape are constrained, we can manage to infer the chemical abundance of the element(s) involved in the transition. The field of stellar atmospheres has seen enormous progress in the last century, from simpler approaches – grey atmospheres, two-level atom – to recent sophisticated 3D models and intensive NLTE calculations. The details on stellar atmospheres and line formation theory are out of the scope of this document – I refer to the textbooks from Mihalas (1970) and Gray (2005) for in-depth discussion and the excellent review from Hubeny (1997) for a summary. I have discussed the basics of stellar atmospheres theory in my Master's Thesis (Puls, 2018).

[3] In this work I am dealing exclusively with absorption lines.

In order to estimate the chemical abundances of species of interest, I propose the classical spectroscopic method as the starting point. This method is outlined in reviews such as those from Allende Prieto (2016), Jofré et al. (2018) and several other works in the literature. Here, I will give a brief summary. The classical method uses 1D LTE atmospheric models, two popular choices being plane-parallel ATLAS9 models (Castelli & Kurucz, 2003) and the spherical MARCS models (Gustafsson et al., 2008). The atmospheric model is needed to solve the radiative transfer equation and to calculate continuum and line formation.

Together with the atmospheric model a well chosen set of spectral lines is required to estimate the column density of each chemical species being studied. In LTE, this involves solving the Boltzmann and Saha equations. Ideally, the lines should be isolated (unblended) and with well determined atomic parameters: lower excitation potential χ, oscillator strength f – the latter is usually tabulated as $\log gf$, g being the statistical weight of the transition.

The choice of unblended lines allows us to measure their equivalent widths (W_λ), whose definition is:

$$W_\lambda = \int_{-\infty}^{+\infty} (1 - F_l(\lambda)/F_c(\lambda))d\lambda, \tag{1}$$

where $F_l(\lambda)$ is the observed line flux and $F_c(\lambda)$ is the continuum flux.

According to curve of growth (CoG) theory of line formation, for weak (unsaturated) lines, whose profile is dominated by thermal broadening, the inferred abundance increases linearly with the logarithm of the measured equivalent width normalized by its wavelength ($\mathrm{RW} = \log_{10}(W_\lambda/\lambda)$). Meanwhile, saturated lines need large abundance changes to imprint changes in W_λ, thus the measurement of weak lines is the most natural choice. It can be deduced from the Maxwellian distribution of velocities that thermal broadening results in a gaussian profile, thus, a gaussian fit reproduces well the unsaturated line. From Eq. 1 it becomes clear that the equivalent width is given by the area of the fitted gaussian[4].

If blending is severe it becomes hard, if not impossible, fitting a gaussian profile on the spectral line of interest. An alternative is to generate a synthetic spectrum and compare it with the observed one. In addition to crowded regions full of blended lines, spectral synthesis is well suited to measurements of molecules and lines affected by hyperfine splitting. However, the need to make a pixel-by-pixel synthesis may introduce non-negligible sources of error, such as variations in the instrumental profile and wavelength calibration (see, e.g., Jofré et al., 2018, and references therein). This is a disadvantage with respect to the equivalent width method, where all

[4]The W_λ is given in units of length, usually mÅ, because the integrand is dimensionless.

information is collapsed in a single value for each line. Finally, both methods suffer from a potentially critical source of error, which is the continuum placement.

2.1.1 The classical method

In Section 2.1 it is said that we need to adopt an atmospheric model to perform the analysis, but, which model? Atmospheric models come in different flavours of geometry (3D, 1D spherical, plane-parallel), physics (LTE/NLTE) and opacity sampling. After choosing the 'flavour', one has to define the input parameters that will define the atmospheric structure of the model (for stratified models, in terms of layer temperature, pressure and other parameters).

For this project, I propose the use of 1D LTE atmospheric models as a starting point, because of their widespread use, relative simplicity and my familiarity with the method (Puls et al., 2018). However, due to the non-equilibrium physics that shapes spectral line formation, one must have in mind that LTE is a very special case of NLTE, the general case (Asplund, 2005). Moreover, the high-precision I am aiming requires to control for as many systematic effects as possible. This includes implementing corrections to 'LTE effects' in abundance values using published grids of NLTE calculations for those species that they are available (e.g., Lind et al., 2011; Bergemann, 2011; Bergemann et al., 2012; Lind et al., 2012; Osorio et al., 2015; Amarsi et al., 2015). Also, the most general treatment *must* account for 3D phenomena: 1D models have the weak assumption that the radiation field is isotropic and they collapse convection – which is intrinsically 3D – into the simplified mixing-length theory.

For 1D LTE models, common input parameters are effective temperature (Teff), surface gravity (usually log g, where g is given in cgs units), metallicity – given in [M/H][5] – and microturbulence (v_t). The model resulting from the input parameters is usually interpolated from a pre-computed grid.

For computing chemical abundances I use the LTE-based code MOOG[6]. It employs 1D atmospheres and CoG theory[7] to calculate chemical abundance from equivalent widths measurements and generates synthetic spectra as well. In the classical spectroscopic method, the input parameters from the atmospheric model are estimated iteratively.

The effective temperature is determined using the *excitation equilibrium*, whose rationale is based on the Boltzmann excitation equation:

[5] Bracket notation for the ratio between overall metallicity and H.

[6] https://www.as.utexas.edu/~chris/moog.html

[7] See the aforementioned textbooks from Mihalas and Gray for in-depth discussion on the CoG theory.

$$\frac{N_{i,r}}{N_i} = \frac{g_r}{\sum_j g_j e^{-\frac{\chi_j}{k_b T}}} e^{-\frac{\chi_r}{k_b T}}, \tag{2}$$

where N_i is the number of atoms of an element in ionization state (species) i and $N_{i,r}$ represents the number of atoms in state i *and* excitation level r, characterized by the lower excitation potential χ_r and the statistical weight g_r. The sum in the right-hand denominator is the partition function. Applying this method implies measuring spectral lines generated in different excitation levels and estimating their $N_{i,r}$. Excitation equilibrium in a slab of gas is reached when the chosen temperature results in the same N_i for all spectral lines considered regardless of the excitation level. That is, the appropriate value of temperature is found then the abundances derived for the lines considered are independent of the lower excitation potential (LEP slope $\rightarrow$ 0).

Assuming hydrostatic equilibrium, the surface gravity is related to the pressure gradient. Since electron pressure is a parameter on the Saha ionization equation, one can apply a rationale similar to excitation equilibrium to find the appropriate value of log g. *Ionization equilibrium* is reached when the model surface gravity yields the same abundance value for different ionization states of the same chemical element[8]. That is, $\Delta I \rightarrow 0$.

The microturbulence v_t affects doppler broadening, and its effect is more intense in strong (RW $\geq$ -5) lines. Basically, it delays the transition between the linear and saturated regimes in the CoG. For instance, if v_t is underestimated, the abundance will be overestimated for the more sensitive stronger lines. The appropriate microturbulence is found when abundances are the same for weaker and stronger lines, i.e, RW slope $\rightarrow$ 0.

For this process, the best suited chemical element in late-type stars is Fe. It has several observable neutral lines in the optical covering large ranges of χ and RW and observable lines from the first ionization state as well. As stressed by Nissen & Gustafsson (2018), a group of lines in a small interval of χ must cover a large range of intensities to avoid degeneracy between Teff and v_t.

Finally, the last input parameter is metallicity, and convergence is reached when inferred and model metallicities are the same ($\Delta M \rightarrow 0$). We must note here that, usually, Fe abundance is used as a proxy for metallicity, but this is only true if the star has solar-scaled composition. On the other hand, there are models suited for α- and C-enhanced stars. One can still use solar-scaled models in those cases if a correction is applied (e.g., Alves-Brito et al., 2010).

Full convergence of the atmospheric parameters is reached when the output parameters vector $\mathbf{o}$ = (LEP slope, ΔI, ΔM, RW slope) is null. The process is iterative and the quantities involved are correlated, thus it

[8]Note that the Saha equation is also temperature-dependent.

can take a long time because MOOG does not have a routine that iterates the atmospheric parameters. One of my ongoing projects is to implement a Python script that reads MOOG output files and uses a numerical method to optimize the process and reach convergence in few (< 10) steps[9].

Having appropriate atmospheric parameters for the star being studied allows the derivation of its detailed chemical composition using CoG theory. Also, it makes possible to build synthetic spectra for those elements unfit for equivalent width analysis.

2.1.2 Differential analysis

Classical spectroscopic analysis, even with well controlled systematics, has limits due to uncertainties in, e.g., atomic parameters such as $\log gf$. For the Sun, Asplund et al. (2009) report uncertainties between 0.04-0.10 dex for each chemical element and this is probably the current lower limit of classical analysis with 'absolute' measurements of chemical abundances. Nissen & Gustafsson (2018) have shown, applying the Cayrel (1988) formula, that for a typical high-resolution (R = 50,000) setup with signal-to-noise ratio (SNR) of 200, the uncertainty in abundance due to the W_λ measurement of an optical line is $\leq$ 0.01 dex, thus, there is room for greater precision if errors in other parameters are cancelled and the observed spectra have high quality. As will be discussed in Section 3, the required precision for my proposal is below 0.04 dex. That is, a differential analysis is required.

As discussed in the review from Nissen & Gustafsson (2018), the differential analysis requires a standard star, imaged with the same setup as the programme stars. Those programme stars have their spectral lines measured with respect to the standard star, which is chosen in a manner that minimizes the systematics in the analysis. That is, both standard and programme stars must have similar atmospheric parameters – ideally, they must be 'twins', so all systematic errors from the atmospheric models cancel out. Then, differential line-by-line analysis allows one to cancel terms related to atomic parameters (see, e.g., Gray, 2005), and to estimate a *differential* abundance of element *El* using only equivalent widths:

$$\delta A(El) = \log \frac{W_{\lambda,P}}{W_{\lambda,S}}. \tag{3}$$

In the above equation, the subscripts P and S refer to 'programme' and 'standard' stars, respectively. If differences in Teff are sufficiently large, a term $-5040\chi/\mathrm{Teff}$ may be added to the right-hand side of Eq. 3. The atmospheric parameters of programme stars are found differentially as well, with excitation and ionization balances, as well as microturbulence fit, being made using differential Fe abundances instead of the 'absolute' ones

[9]Each iteration of the MOOG *abfind* module usually takes less than one second in an average laptop.

(see, e.g., Meléndez et al., 2014). When the stars are not twins, full excitation/ionization balance or microturbulence fit may be relaxed up to some point, as in Alves-Brito et al. (2010). The atmospheric parameters of the standard star may be constrained by measurements made through non-spectroscopic methods, e.g., interferometry or asteroseismology, if they are available.

If one is interested in a comparison between sets of stars of different regions of the atmospheric parameters space, the respective standard stars may be analysed with a more realistic model (e.g., full 3D, NLTE) and the differential abundances may be converted to 'absolute' ones, using those 'absolute' abundances calculated for the standard star through the more realistic model (Nissen & Gustafsson, 2018). However, there are situations where we are interested in a strict differential analysis of similar stars (e.g., the [Y/Mg] clock for solar twins) and the estimation of 'absolute' abundances is not necessary.

2.2 Asteroseismology

Asteroseismology is the study of the properties of stars, both internal and global, through their photometric oscillations (Hekker & Christensen-Dalsgaard, 2017). Here, I am interested in *solar-like oscillations*, thought to be excited and damped by near-surface turbulent convection, the same mechanism driving helioseismological phenomena. These oscillations are supposed to happen in stars with convection in their outer layers – that is, not only main sequence FGK stars, but also stars in the Sub-Giant Branch (SGB) as well as those in the RGB and those passing through the Core He-Burning phase (CHeB) (see, e.g., Houdek et al., 1999; Samadi & Goupil, 2001).

The power spectrum of solar-like oscillators is characterized by a series of peaks modulated by a gaussian envelope (Chaplin & Miglio, 2013). From the power spectrum we can extract the two main asteroseismological quantities of interest in this project, $\Delta\nu$ and $\nu_{\max}$. In the case of p-modes – i.e. those where pressure is the restoring force, $\Delta\nu$ is the average frequency spacing between such peaks of same angular degree l and consecutive radial orders n. In the first order, the individual frequencies in the power spectrum are given by:

$$\nu_{nl} \sim \Delta\nu \left(n + \frac{l}{2} + \epsilon \right) \tag{4}$$

where ϵ is a constant. This is valid in the asymptotic limit where $l/n \to 0$ (Christensen-Dalsgaard & Houdek, 2010). It is worth remarking that $\Delta\nu$, as an average parameter, does not take into account higher order effects. For instance, to interpret the power spectrum of solar-like oscillations, one must take into account the small frequency separation $\delta\nu$, which breaks the degeneracy $\nu_{nl} \approx \nu_{n+1,l-2}$ cointained in Eq. 4. These higher order effects

trace spatial strucutural changes in the stellar interior and are more intense in evolved stars (Chaplin & Miglio, 2013).

It can be shown, using linear adiabatic theory, (e.g., Kjeldsen & Bedding, 1995) that $\Delta\nu$ is proportional to the square root of the star's mean density. Scaling the relationship with respect to the Sun, we may write:

$$\frac{\Delta\nu}{\Delta\nu_\odot} \simeq \left(\frac{\overline{\rho}}{\overline{\rho}_\odot}\right)^{\frac{1}{2}} = \left(\frac{M}{M_\odot}\right)^{\frac{1}{2}} \left(\frac{R}{R_\odot}\right)^{-\frac{3}{2}} \tag{5}$$

The frequency of maximum oscilation power $\nu_{\max}$ is tought to scale with the maximum acoustic cut-off frequency, which traces near-surface structure. Its relation with global stellar parameters such as effective temperature and surface gravity is (e.g., Brown et al., 1991; Kjeldsen & Bedding, 1995):

$$\nu_{\max} \propto gT\mathrm{eff}^{-\frac{1}{2}} \tag{6}$$

Scaling $\nu_{\max}$ to the solar value and rearranging Eqs. 5 and 6, we obtain the asteroseismic scaling relations:

$$\begin{aligned}
\frac{M}{M_\odot} &\simeq \left(\frac{\nu_{\max}}{\nu_{max,\odot}}\right)^{3} \left(\frac{\Delta\nu}{\Delta\nu_\odot}\right)^{-4} \left(\frac{T_{\rm eff}}{T_{\rm eff,\odot}}\right)^{\frac{3}{2}} \\
\frac{R}{R_\odot} &\simeq \left(\frac{\nu_{\max}}{\nu_{max,\odot}}\right) \left(\frac{\Delta\nu}{\Delta\nu_\odot}\right)^{-2} \left(\frac{T_{\rm eff}}{T_{\rm eff,\odot}}\right)^{\frac{1}{2}} \\
\log g &\simeq \log\frac{\nu_{\max}}{\nu_{max,\odot}} + \frac{1}{2}\log\frac{T_{\rm eff}}{T_{\rm eff,\odot}} + \log g_\odot
\end{aligned} \tag{7}$$

As shown in Eq. 7, from the observed quantities $\Delta\nu$ and $\nu_{\max}$, one can estimate fundamental parameters of the star such as mass, radius and surface gravity. **For red giants, mass is a good proxy for age**[10], due to the much smaller lifetime with respect to main-sequence lifetime. Thus, asteroseismology can be a very useful tool to infer stellar ages of red giants, with implications for Galactic archaeology (Miglio et al., 2013; Stello et al., 2015; Casagrande et al., 2016).

Solar-like oscillations may be detected both by photometry and radial velocity campaigns. However, before the launch of space-based observatories specialized in high-precision photometry such as CoRoT and Kepler, only a handful of nearby stars other than the Sun had $\Delta\nu$ and $\nu_{\max}$ measurements (e.g. Gilliland, 2008; Stello et al., 2008). Nowadays, we can take advantage of the large dataset provided by space-based missions – the Kepler mission alone has detected solar-like oscillations in thousands of red giants (see Yu et al., 2018, and references therein) with the part-per-million precision required for detections (Huber et al., 2011a).

[10] Assuming no mass transfer from/to another stellar object and/or negligible mass loss.

The data under study is discrete and needs to be transformed to Fourier space, and, in principle, it is subject to the Shannon-Nyquist theorem (but see, e.g., Murphy et al., 2013; Chaplin et al., 2015). This implies that the maximum usable frequency B is $B \leq F_s/2$, where F_s is the sampling frequency. Both Kepler and K2 missions gather their photometry in short- (1 minute) and long- (30 minutes) cadence modes (Chaplin & Miglio, 2013). While long-cadence mode is not suited for $\nu_{\rm max}$ measurements of main-sequence stars, it allows the study of red giants whose log g is above $\sim$ 3.3 dex. Regarding $\Delta\nu$, frequency resolution is decisive. For a low-mass star on the RGB-tip, $\Delta\nu \sim 0.5$ μHz (Casagrande et al., 2014; Mathur et al., 2016; Yu et al., 2018). Assuming $\Delta\nu_{min} = F_s/N$, with N being the number of data points, $\sim$ 24 days of continuous observations are required, roughly the duration of CoRoT 'short runs' (Deleuil et al., 2011). The duration of each K2 campaign is $\sim$ 75 days (Howell et al., 2014), while the Kepler dataset has observations that extend through hundreds or thousands of days, depending on the target.

Another caveat when considering the asteroseismical parameters is that scaling relations, while derived from first principles, assume that all stars are homologous to the Sun and do not account for nonlinear effects (see, e.g., Mosser et al., 2013). Studies of binary systems with independently measured masses show that 'pure' asteroseismical scaling relations overestimate the fundamental stellar parameters of red giants, up to 20 % in the case of stellar masses (Gaulme et al., 2016; Brogaard et al., 2018). An alternative is to apply correction factors to the scaling relations, such as those calculated by, e.g., Rodrigues et al. (2017). A complementary approach is grid-based modelling, where the observed $\Delta\nu$ and $\nu_{\rm max}$ are used as input to retrieve fundamental quantities from a large grid of stellar models (see Stello et al., 2009; Chaplin et al., 2014; Serenelli et al., 2017, for examples). Other alternative method is individual frequency modelling (e.g. Kallinger et al., 2008). As of today, the use of scaling relations together with grid-based modelling is the standard procedure.

It is worth remarking that the analysis of solar-like oscillations is powerful enough to differentiate between giants in the H-shell burning phase and those in the CHeB phase. Bedding et al. (2011) developed a method to differentiate stars in the red clump using mixed modes, i.e., those which result from coupling between p-mode and g-mode oscillations. The g-modes are characterized by having buoyancy as restoring force, constant separation in *period* and manifest themselves in non-radial ($l \neq 0$) degrees.

Through the use of scaling relations, one can employ asteroseismic observations to estimate surface gravity. Taking into account the above discussed points regarding accuracy and with a Teff determined by the InfraRed Flux Method (IRFM), the precision in log g is of the order of 0.01 dex or even less (e.g., Casagrande et al., 2014). This level of precision may help to constrain the value of surface gravity used as input in model atmospheres for

a differential analysis. However, it must be emphasized that, due to the asteroseismical log g dependence on Teff, a poorly determined effective temperature will propagate the error to asteroseismological surface gravity. This may affect the determination of the other atmospheric parameters – due to their correlations – and, obviously, the derived chemical abundances.

3 Proposed work

As outlined in Section 1.1, the main purpose of this project is the search and characterization of the [Y/Mg]-age relation and other potential chemical clocks such as the [Y/Al] and [Ba/Mg] ratios. I intend to take advantage of the large datasets from Kepler and K2 and their thousands of published $\Delta\nu$ and $\nu_{\rm max}$ values. These large datasets will allow building a sample of targets with relatively precise masses and ages.

In short, the proposed work is organized as follows. Project 1 will follow up previous studies of stars whose chemistry and asteroseismological ages do not match. One of my goals is to acquire knowledge and experience in asteroseismology, and finishing my PhD being skilled in more than one area – in this sense, Project 1 will work as a training ground while new data is not available yet. Later, its results will be put in the context that, I expect, will be offered by Project 2, where I intend to investigate chemical clocks with fine detail, potentially unveiling details in a small-scale level. Finally, there is Project 3: I intend to conduct an analysis similar to that of Project 2 in open cluster stars, where they work as a control group. This is due to the fact that we do not need to rely on asteroseismology to infer relatively precise ages for open clusters. The control group would allow the detection of possible bias or systematics in asteroseismological ages.

3.1 Project 1: chemically unusual stars

Besides the study of chemical clocks themselves and their impact in the study of Galactic evolution, there is a puzzle where they may be helpful. Stars with 'unexpected' chemistry with respect to their ages have been detected in both Kepler and CoRoT fields (Martig et al., 2015; Chiappini et al., 2015). They come in different flavours: young α-rich, young metal-poor and old metal-rich stars. While these results may contradict the expectations from Galactic chemical evolution – e.g., the [α/Fe] ratio is supposed to decrease with the onset of Type Ia SNe – Epstein et al. (2014) detected masses systematically higher than expected for halo and thick-disc stars. This raised the question that scaling relations may be unfit for certain metallicity regimes, while more recent works have reached good accuracy after applying correction factors, as discussed in Section 2.2.

One possible explanation is that at least some of these unusual stars – the young α-rich – would be blue stragglers (Yong et al., 2016; Jofré et al.,

2016; Matsuno et al., 2018). This would imply that, in these cases, the high masses measured through scaling relations would be the result from a merger event and would be masking their true ages. This may be the case for the young metal-poor targets as well. To investigate that and the nature of the old metal-rich ones, we are conducting a spectroscopic analysis to characterize their *detailed* chemical composition. This sample contains 23 targets from the Kepler field and was observed with HIRES@Keck (Vogt et al., 1994). Besides these 23 stars from the Kepler field, 6 stars studied by Alves-Brito et al. (2010) (5 from the red clump) were also observed to provide a link to past chemical studies. Finally, 3 standard stars (HD 146233, HD 122563, HD 140283) complete the sample, all observed in the same run with HIRES@Keck. The 23 stars from the Kepler field span a wide range of atmospheric parameters – 4200 K $<$ Teff $<$ 5200 K; 1.0 $<$ log g $<$ 3.4; -2.3 $<$ [Fe/H] $<$ 0.2. Thus, a strict differential analysis of the *entire* sample is not possible, but some of its members may be clustered in subgroups for differential analysis if this is considered useful.

The data are already reduced and a chemical analysis whose method is similar to that adopted by Valentini et al. (2018) is ongoing. Basically, IRFM and asteroseismic values of log g will be employed to constrain the atmospheric parameters for the classical analysis (explained in Section 2.1.1). The choice of not using excitation/ionization equilibria comes from the expected lower precision of the classical approach. Because asteroseismic log g is Teff-dependent, IRFM Teff is (mildly) metallicity-dependent, the process to determine the atmospheric parameters will still be iterative. Here, the main difference is that Fe II lines may be ignored (they are only needed for ionization equilibrium), but, still, a full classical determination of atmospheric parameters will be interesting for comparison. Then, using the interpolated atmospheric model, MOOG calculates LTE chemical abundances from measured spectral lines straightforwardly.

Some targets in this sample – mostly the metal-poor ones – are expected to be severely affected by 'LTE effects', and corrections to NLTE regime will be applied when available. I intend to implement an algorithm that applies the correction directly on MOOG. We have plans for an 1 month visit to asteroseismology experts where I will learn in detail methods of light-curve analysis and grid-based modelling, complementing the spectroscopic analysis, and enabling the inference of refined values of ages from asteroseismology for the subset from the Kepler field directly from their light curves. This would be helpful not only for the present work, but to be prepared for future data releases from missions such as TESS and PLATO, to be used in post-PhD works.

Expected outcomes: With a detailed chemical analysis we may try to detect signatures of mass transfer (if any) in the supposed blue stragglers. Also, if the search for chemical clocks results in an age-[Fe/H]-$[A/B]_{clock}$ grid (discussed in Section 3.2), it may be possible to use this detailed chemical

analysis to infer the ages of (at least some of) these supposed young metal-poor and α-rich stars and check if they are the result of a merger or a mass transfer with a method independent of, e.g., radial velocity variations. The study of potential outliers is useful to check their behaviour with respect to chemical clocks. It might give us a additional method to identify unusual stars.

3.2 Project 2: chemical clocks in field stars

As previously discussed, Feltzing et al. (2017) have shown that the [Y/Mg] clock should work if one controls [Fe/H], while Slumstrup et al. (2017) have detected it for a small (N=6) sample of CHeB stars. Thus, I propose dividing a large sample in subsets of relatively narrow (δ[Fe/H] $\leq$ 0.3 dex) bins. This bin width is based on the results from Nissen (2015), who found the [Y/Mg] clock in a sample of solar twins where -0.15 $<$ [Fe/H] $<$ 0.15. Then, with respect to metallicity, we can investigate:

- If the [Y/Mg]-age relation holds for red giants in metallicity regimes besides solar;
- If the slope of the chemical clock – if found – is metallicity-dependent;
- How other abundance ratios – e.g., [Ba/Mg] – behave with respect to metallicity and age.

In the case of elements with nucleosynthetic metallicity-dependent yields, one should expect that the potential chemical clocks involving these elements would display different behaviours in distinct metallicities. If this is observationally confirmed, it may be possible to build an empirical 3D age-[Fe/H]-[A/B]$_{\rm clock}$ grid instead of a simple 2D age-[A/B]$_{\rm clock}$ relation. The existence of a grid based on abundance ratios extensively tested would be an independent method for age determination, and, coupled with asteroseismology, useful to, e.g., identify blue stragglers in the field, as could be the case for some stars from Project 1.

However, due to different timescales and chemical evolution involved, we must also control for Galactic environment. Data from Gaia DR2 may be used to constrain thin-disc, thick disc or halo membership – using, for instance, a Toomre diagram (e.g. Bensby et al., 2014). For those targets not among the 7×10^6 objects having full 6D state vectors from Gaia DR2 (Marchetti et al., 2018), heliocentric radial velocity may be measured from the observed spectrum.

A possible variable control for stellar evolution effects is the measurement of chemical clocks in different regions of the HRD. The sample may be constituted by subsets in different bins of surface gravity: $\log g \sim 1.6$ (Arcturus analogs), and those in the luminosity region of the red and secondary

clumps (for details on the red clump, see the review from Girardi, 2016). We can take advantage of asteroseismic information to break the degeneracy between CHeB and ascending-RGB stars in the HRD, as discussed in Section 2.2. Therefore, it is possible to have n+1 subsets of stars in different evolutionary phases, n being the number of HRD regions with observations. The bin width that I suggest for log g is 0.3 dex, corresponding to 1-σ in the classical spectroscopic approach.

The chemical abundances will be determined using strict differential analysis (discussed in Section 2.1.2), as the required precision in [Y/Mg] and other chemical clocks for a expected age resolution of 1 Gyr is 0.04 dex, based on solar twin studies. The atmospheric parameters will be constrained again by asteroseismic log g and photometric Teff, but estimated differentially with respect to the chosen standard star. To minimize systematics introduced by 'LTE effects', NLTE corrections will be employed even in solar metallicity regime, where they are expected to be mild. The reason is that – at the expected precision – even 'LTE effects' with magnitudes of 0.01-0.02 dex may change the slope of the age-abundance fit, if they are not homogeneous along the sample.

Expected outcomes: Regarding the abundance ratios trend, based on solar twins studies I expect a negative correlation between age and [s/α], where 's' accounts for s-process elements such as Y and Ba. The slope of the correlation is expected to change from a s-process element to another depending on the stellar mass where the respective s-process elements production peak[11]. As previously discussed, I expect to find a high-precision grid of abundance ratios tightly correlated with ages in narrow metallicity bins, with implications to the study of the chemical evolution of the Galaxy and (potentially) to stellar evolution.

The material for publication may be divided in a series of papers, each one describing the results in a single metallicity bin, or a single region of the HRD, or a single Galactic component. The way I will organize the series of publications depends on the dataset I will have. At the moment, I am not aware of high quality, collected homogeneously, archival spectra of field stars with published asteroseismic parameters in a quantity high enough to explore the details I described in this Section. If this does not change, I will have to rely on new observations for Project 2.

3.2.1 Potential dataset

In this section I will outline the potential use of Kepler and K2 data and how I intend to use them as a starting point for target selection. I will briefly describe the observational limitations to take into account when writing an observing proposal for this work.

[11] Here I am referring to the masses of stars that enriched the interstellar medium before the formation of those stars I intend to observe.

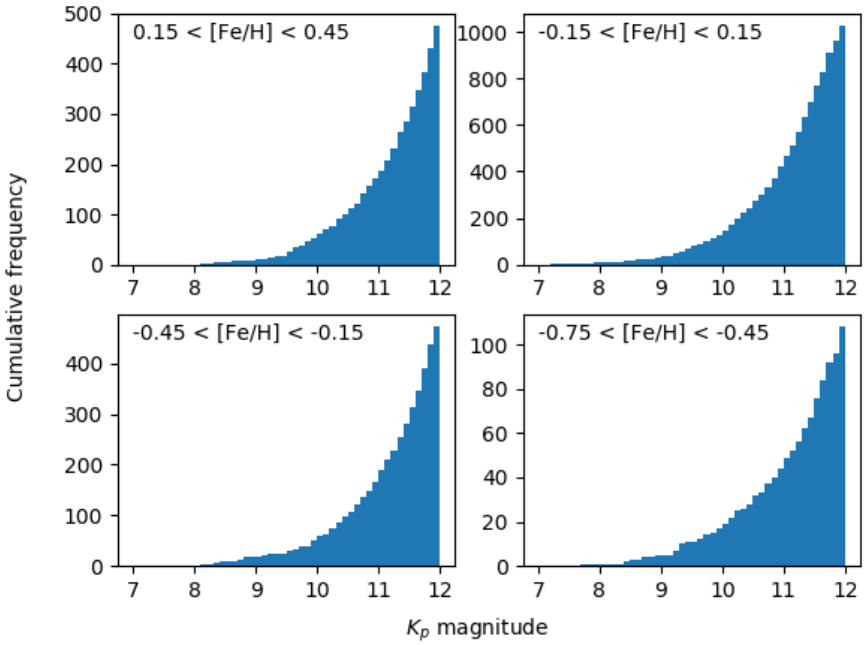

Figure 2: Cumulative distributions of magnitudes up to $K_p = 12$ of stars from the Kepler field with clump-like surface gravities – $2.4 < \log g < 2.7$ – and solar-like oscillations detected by Yu et al. (2018).

The Kepler mission observed more than 196,000 stars. Of these, $\sim$ 19,000 red giants had solar-like oscillations detected (Hekker et al., 2011; Huber et al., 2011b; Stello et al., 2013; Huber et al., 2014; Mathur et al., 2016; Yu et al., 2016, 2018). Before submitting an observing proposal, we must have an idea of the sample size. A simple estimation may be made as follows.

For the Kepler field (RA: 19h20m, Dec: +45 deg), it is obvious that the chosen observatory must be located in the northern hemisphere, and the optimal observing month is July. Possible instruments are HIRES@Keck, HDS@Subaru (Noguchi et al., 2002), and GRACES@Gemini (Chene et al., 2014). Estimating exposure times for HIRES with standard inputs, a 3600 s exposure is sufficient for SNR per pixel of 200 at the 600 nm region of a $V = 12.5$ K-type star. HDS exposure calculator gives similar performance, while GRACES maximum exposure time (2400 s) is sufficient[12].

Using the photometric calibrations described by Brown et al. (2011), a relationship between Kepler magnitudes (K_p) and the Johnson system may

[12]Of course, these are only initial estimations, and multiple exposures may be used for fainter objects if it is the case. Also, brighter objects may be chosen, if possible, to achieve higher SNR values.

be derived:

$$\begin{aligned} K_p &= V - 0.244(B-V) + 0.082,\ (B-V) \leq 1 \\ K_p &= V - 0.342(B-V) + 0.101,\ (B-V) > 1 \end{aligned} \tag{8}$$

From the relations in Eq. 8, a conservative estimation for K-type giants is $K_p = V - 0.5$, implying a $K_p = 12$ upper limit for stars in the Kepler catalog if a maximum exposure time of 3600 s per target for SNR $\approx$ 200 is imposed.

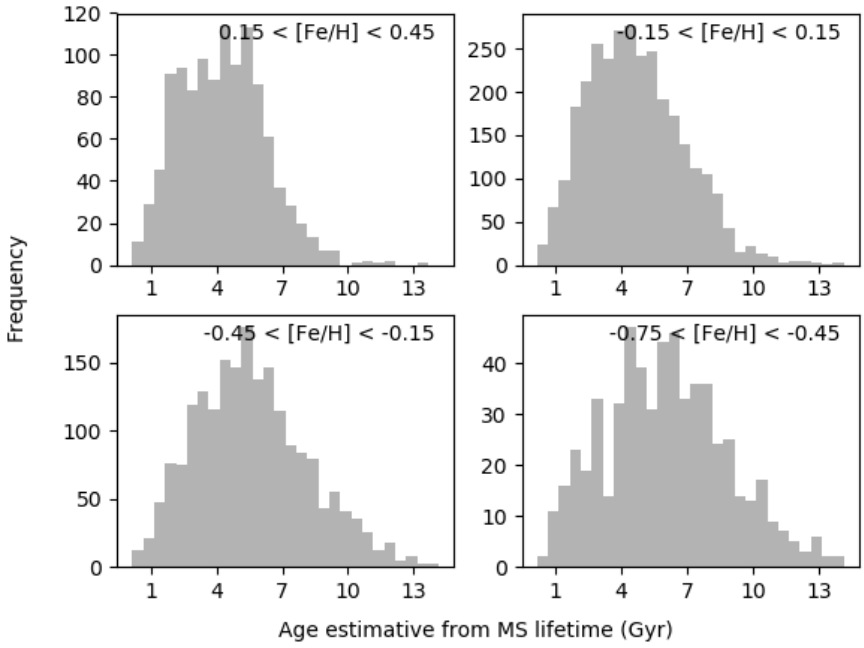

Figure 3: Estimated age distribution for the subset shown in Fig. 2. Note: the values are a *very rough* estimation from the main-sequence lifetime equation $\tau_{\rm MS} \propto (M/M_\odot)^{-2.5}$.

Using the catalog from Yu et al. (2018) (N=16,094) to identify red giants with solar-like oscillations, it is possible to find 4452 red giants with $K_p < 12$. Of these, 1730 have $K_p < 11$. In Fig. 2 the cumulative distribution of magnitudes is shown for potential targets with surface gravities typical of red clump stars, divided in metallicity bins.

In Fig. 3, the age distribution of the same subset of stars is shown. **These ages are not intended to be accurate**: they were inferred by the main-sequence lifetime equation $\tau_{\rm MS} \propto (M/M_\odot)^{-2.5}$ just to show a rough approximation of shape of the true age distribution. Grid-based modelling is supposed to yield more accurate ages. Anyway, the distributions shown

in Fig. 3 reflect the fact that the bulk of the subset under consideration has masses between 1-2 $M_{\odot}$, as inferred by Yu et al. (2018).

Figs. 2 and 3 indicate that a careful choice of targets may yield a good age (mass) distribution for the analysis of the chemical clocks. Apart from the more metal-poor bin, Fig 2 suggests that it is feasible to limit target choice to $K_p < 10.5$ ($V \approx 11$), but a careful analysis of the age (mass) distribution with respect to apparent magnitude needs to be done in order to confirm this.

While most of the red giant subset is concentrated in the red clump region of the HRD, some of the objects catalogued by Yu et al. (2018) are not. If we consider stars with surface gravities similar to Arcturus ($1.5 < \log g < 1.8$), 155 have $K_p < 12$. The distribution of these 155 objects through the same metallicity bins adopted for clump-like stars is 16, 82, 36 and 18, in decreasing order of [Fe/H].

Taking into account that the analysis from Nissen (2015) was done with 21 targets, in the worst case scenario (3600 s/target) a sample of similar size would take 2-3 observing nights to have images acquired – for each bin of metallicity and atmospheric parameters. Therefore, it may be possible to do most of the work (including some open clusters) only using stars observed by the Kepler mission, if enough observing time is granted.

Nevertheless, the K2 mission has observations of several regions of the ecliptic plane – a total of 19 campaigns, covering an area of the sky much larger than the Kepler mission. It also allows the use of instruments in the southern hemisphere, such as UVES@VLT (Dekker et al., 2000).

Applying the same filter used to select the subset from Fig. 2 to the EPIC catalog (Huber et al., 2017), a total of 5138 objects with the flag 'observed' (by K2) are listed. Some of them have asteroseismological parameters published by the K2 Galactic Archaeology Program (K2GAP) DR1 (Stello et al., 2017). The K2GAP identified a total of 1200 red giants with solar-like oscillations in Campaign 1 (C1) of K2. The C1 field is near the celestial equator and its optimal observing month is March (RA: 11h35m46s, Dec: +01d25m02s).

Cross-matching the K2GAP DR1 and EPIC catalogs and applying the same filters used for the analysis of the Kepler field, there are 35, 62 and 20 potential targets with clump-like gravities for the [Fe/H] bins centered at 0.00, -0.30 and -0.60, respectively. Their distance moduli $(V - M_V) > 9$ and location on the North Galactic Cap suggest that at least some of these stars do not belong to the thin disc, thus, a careful kinematic analysis is needed before submitting a proposal. Unfortunately, few (3) objects with $\log g$ close to the Arcturus value had solar-like oscillations detected by Stello et al. (2017), therefore the analysis of a K2 sample would probably focus only in stars with clump-like gravities. I must remark that the discussion made about the K2 sample is taking into account only the C1 field of K2, and further data releases from the K2GAP for other K2 campaigns may help

to expand the number of potential targets.

Also, it is possible to take an inverted path to acquire the required data for the analysis. That is, archive-mining for homogeneous sets of high-quality spectra, complemented by light-curve analysis of K2 and CoRoT red giants without values of $\Delta\nu$ and $\nu_{\rm max}$ published to date. Or, even, focus on light curve analysis of chosen targets. I intend to acquire the required know-how for this inverted path until the end of the current year. The invitation of other collaborators to help in both the analysis and observations is being considered as well.

3.3 Project 3: open clusters

Bossini et al. (2019) estimated ages for 269 open clusters through isochrone fitting using Gaia DR2 parallaxes and kinematics, claiming typical 16th-84th confidence intervals of 50 Myr. Spectra from open cluster stars with well determined ages may add a further constrain independent of asteroseismology to chemical clocks.

While it is interesting to investigate dwarfs or MSTO stars here, the use of red giants may extend the observational limit due to their greater luminosities. But, primarily, it works as a control group for Project 2, because their ages, here, do not rely on $\Delta\nu$ and $\nu_{\rm max}$. This limits minimum age to be considered as that when the cluster already has a minimum number of red giants. The number may be set to 4 (Hyades, age $\approx$ 625 Myr). From Bossini et al. data, setting the distance modulus of NGC 6791[13] (V-M$_V$ = 13.085) as an upper spatial limit, there are 40 open clusters older than the Hyades, 16 having metallicities already determined with high-resolution spectroscopy.

A possibility here is to extend the work from Slumstrup et al. (2017) for other clusters and abundance ratios other than [Y/Mg]. I expect to find a sufficient number of high quality archival spectra from open clusters, because several are well studied objects (e.g., Hyades, M 67). Otherwise, I will need to apply for observing time again, but, this time, without being limited to northern hemisphere observatories as in the Kepler field or constrained to stars with high-precision light curves.

Expected outcomes: This project, working as a control group, is expected to validate the results obtained with ages determined by asteroseismology. If the outcomes of Projects 2 and 3 are different, the potential implication is a divergence on different age-determination methods. Thus, if that is the case, this work would give a motivation to the community to work to improve these methods.

Summarizing, there is enough work for several publications in this proposal. The search for chemical clocks can be divided in a series of papers,

[13]The oldest open cluster, 8.4 Gyr.

each one testing a control variable: different [Fe/H] bins, individual regions of the HRD, the investigation of different Galactic environments and the open clusters. The study of chemically unusual stars should be the first publication, as the investigation is ongoing.

As a bonus, I am implementing several algorithms in Python that deal with several steps along data reduction and spectroscopic analysis. I see that as extremely important because IRAF, which has been an informal 'standard' in astronomical data analysis in past decades, is being discontinued. Python is open, easy to install and to execute as a cross-platform language, so it seems an obvious choice to me. I intend to release the tools under development to usage by anyone eventually interested.

3.4 Back-up projects (where data are already in hand)

The work on the [Y/Mg] and other chemical clocks may depend, to a good extent, on new data. This implies relying on observing proposals for telescope time that may be accepted or rejected. In the case of an eventual rejection for observing time, there are some alternative topics which also interest me and may work as parallel projects. Of course, this is only a list of proposals, and new ideas for parallel projects may appear as my knowledge of both astronomy and resources available in archives grow:

- Reanalysis of M 4 and M 5 spectra from Yong et al. (2008). Their high SNR (> 200) would allow a differential analysis that may identify (or not) unknown inhomogeneities. An interesting information related to Project 1 arising from Yong et al. (2008) findings is a difference of 0.33 dex between the [Y/Mg] ratios from M 4 and M 5. This is due to the fact that M 4 has enhancement in s-process elements. Taking into account their similar metallicity and similar ages (from [Th/Eu]), this suggests that the [Y/Mg] clock does not work for globular clusters, and/or for environments older than the thin disc.

- Inhomogeneities in open clusters. Liu et al. (2016) and Spina et al. (2018) have found 0.02 dex-level chemical inhomogeneities in the Hyades and Pleiades, with potential implications for chemical tagging (Freeman & Bland-Hawthorn, 2002). I am aware of the existence of high quality datasets from collaborators of our group for three other open clusters where a similar analysis may be done – but I need to check their status. Also, Liu et al. (2019) found no clear inhomogeneities in M 67, while their results may indicate effects of atomic diffusion, another interesting topic.

3.5 Proposed timeline

Mar-Jun 2019:

- Familiarise myself with the asteroseismology of solar-like oscillators;
- Start the analysis of chemically unusual stars;
- Start the thesis proposal.

Jul-Dec 2019:

- Present the thesis proposal talk;
- Visit another institution to learn advanced methods in asteroseismology;
- Submit a proposal for targets in the Kepler field;
- Finish the analysis of chemically unusual stars and start the manuscript for the first publication.

Jan-Jun 2020:

- (If accepted) observe targets in the Kepler field and/or in K2 C1 field;
- (Otherwise) Submit new proposal for Kepler (and K2) field and start a parallel project if possible;
- Attend a conference to present the work on chemically unusual stars.

Jul-Dec 2020:

- Data reduction of any remaining raw data and subsequent spectroscopic analysis for Projects 1 and 2;
- Fine-tune previous published asteroseismological analysis for observed targets;
- Submit new observing proposal, if required;
- Carry on parallel projects, if possible;
- Attend a conference to present work.

2021:

- Analysis of the observed data: separate investigations in bins of atmospheric parameters, Galactic components and the open cluster control group;
- Start manuscripts for publications;
- Carry on parallel projects, if possible;

- Attend conferences to present work.

2022:

- Submit any remaining manuscripts;
- Attend conferences to present work;
- Start writing the thesis and give final thesis talk.

References

Allende Prieto C., 2016, Living Reviews in Solar Physics, 13, 1

Alves-Brito A., Meléndez J., Asplund M., Ramírez I., Yong D., 2010, A&A, 513, A35

Amarsi A. M., Asplund M., Collet R., Leenaarts J., 2015, MNRAS, 454, L11

Asplund M., 2005, ARA&A, 43, 481

Asplund M., Grevesse N., Sauval A. J., Scott P., 2009, ARA&A, 47, 481

Baglin A., et al., 2006, in 36th COSPAR Scientific Assembly. p. 3749

Bedding T. R., et al., 2011, Nature, 471, 608

Bensby T., Feltzing S., Oey M. S., 2014, A&A, 562, A71

Bergemann M., 2011, MNRAS, 413, 2184

Bergemann M., Lind K., Collet R., Magic Z., Asplund M., 2012, MNRAS, 427, 27

Bland-Hawthorn J., Gerhard O., 2016, Annual Review of Astronomy and Astrophysics, 54, 529

Borucki W. J., et al., 2008, in A Decade of Extrasolar Planets around Normal Stars Proceedings of the Space Telescope Science Institute Symposium. pp 36–49

Bossini D., et al., 2019, A&A, 623, A108

Brogaard K., et al., 2018, MNRAS, 476, 3729

Brown T. M., Gilliland R. L., Noyes R. W., Ramsey L. W., 1991, ApJ, 368, 599

Brown T. M., Latham D. W., Everett M. E., Esquerdo G. A., 2011, AJ, 142, 112

Butcher H. R., 1987, Nature, 328, 127

Cardelli J. A., Clayton G. C., Mathis J. S., 1989, ApJ, 345, 245

Casagrande L., et al., 2014, ApJ, 787, 110

Casagrande L., et al., 2016, MNRAS, 455, 987

Castelli F., Kurucz R. L., 2003, in Piskunov N., Weiss W. W., Gray D. F., eds, IAU Symposium Vol. 210, Modelling of Stellar Atmospheres. p. A20 (arXiv:astro-ph/0405087)

Cayrel R., 1988, in Cayrel de Strobel G., Spite M., eds, IAU Symposium Vol. 132, The Impact of Very High S/N Spectroscopy on Stellar Physics. p. 345

Chaplin W. J., Miglio A., 2013, Annual Review of Astronomy and Astrophysics, 51, 353

Chaplin W. J., et al., 2014, ApJS, 210, 1

Chaplin W. J., et al., 2015, PASP, 127, 1038

Chene A.-N., et al., 2014, in Proc. SPIE. p. 915147 (arXiv:1409.7448), doi:10.1117/12.2057417

Chiappini C., et al., 2015, A&A, 576, L12

Christensen-Dalsgaard J., Houdek G., 2010, Ap&SS, 328, 51

Connelly J. N., Bizzarro M., Krot A. N., Nordlund Å., Wielandt D., Ivanova M. A., 2012, Science, 338, 651

Cristallo S., Straniero O., Piersanti L., Gobrecht D., 2015, ApJS, 219, 40

De Silva G. M., et al., 2015, MNRAS, 449, 2604

Dekker H., D'Odorico S., Kaufer A., Delabre B., Kotzlowski H., 2000, in Iye M., Moorwood A. F., eds, Society of Photo-Optical Instrumentation Engineers (SPIE) Conference Series Vol. 4008, Proc. SPIE. pp 534–545, doi:10.1117/12.395512

Deleuil M., Moutou C., Bordé P., 2011, in European Physical Journal Web of Conferences. p. 01001 (arXiv:1105.1887), doi:10.1051/epjconf/20101101001

Delgado Mena E., et al., 2019, A&A, 624, A78

Dotter A., Sarajedini A., Anderson J., 2011, ApJ, 738, 74

Edvardsson B., Andersen J., Gustafsson B., Lambert D. L., Nissen P. E., Tomkin J., 1993, A&A, 500, 391

Epstein C. R., et al., 2014, ApJ, 785, L28

Feltzing S., Holmberg J., Hurley J. R., 2001, A&A, 377, 911

Feltzing S., Howes L. M., McMillan P. J., Stonkutė E., 2017, MNRAS, 465, L109

Feuillet D. K., et al., 2018, MNRAS, 477, 2326

Freeman K., Bland-Hawthorn J., 2002, ARA&A, 40, 487

Gaia Collaboration et al., 2016, A&A, 595, A1

Gaia Collaboration et al., 2018, A&A, 616, A1

Gaulme P., et al., 2016, ApJ, 832, 121

Gilliland R. L., 2008, AJ, 136, 566

Gilmore G., et al., 2012, The Messenger, 147, 25

Girardi L., 2016, ARA&A, 54, 95

Gray D. F., 2005, The Observation and Analysis of Stellar Photospheres

Gustafsson B., Edvardsson B., Eriksson K., Jørgensen U. G., Nordlund Å., Plez B., 2008, A&A, 486, 951

Harris W. E., 1996, AJ, 112, 1487

Harris W. E., 2010, arXiv e-prints, p. arXiv:1012.3224

Haywood M., Di Matteo P., Lehnert M. D., Katz D., Gómez A., 2013, A&A, 560, A109

Hekker S., Christensen-Dalsgaard J., 2017, A&A Rev., 25, 1

Hekker S., et al., 2011, MNRAS, 414, 2594

Houdek G., Balmforth N. J., Christensen-Dalsgaard J., Gough D. O., 1999, A&A, 351, 582

Howell S. B., et al., 2014, PASP, 126, 398

Howes L. M., Lindegren L., Feltzing S., Church R. P., Bensby T., 2019, A&A, 622, A27

Hubeny I., 1997, Stellar Atmosphers Theory: an Introduction. p. 1, doi:10.1007/BFb0113481

Huber D., et al., 2011a, ApJ, 731, 94

Huber D., et al., 2011b, ApJ, 743, 143

Huber D., et al., 2014, ApJS, 211, 2

Huber D., Bryson S. T., et al. 2017, VizieR Online Data Catalog, p. IV/34

Jofré P., et al., 2016, A&A, 595, A60

Jofré P., Heiter U., Soubiran C., 2018, arXiv e-prints, p. arXiv:1811.08041

Kallinger T., et al., 2008, A&A, 478, 497

Karakas A. I., Lattanzio J. C., 2014, PASA, 31, e030

Karakas A. I., Lugaro M., 2016, ApJ, 825, 26

Kjeldsen H., Bedding T. R., 1995, A&A, 293, 87

Kobayashi C., Umeda H., Nomoto K., Tominaga N., Ohkubo T., 2006, ApJ, 653, 1145

Leaman R., VandenBerg D. A., Mendel J. T., 2013, MNRAS, 436, 122

Lind K., Asplund M., Barklem P. S., Belyaev A. K., 2011, A&A, 528, A103

Lind K., Bergemann M., Asplund M., 2012, MNRAS, 427, 50

Liu F., Yong D., Asplund M., Ramírez I., Meléndez J., 2016, MNRAS, 457, 3934

Liu F., Asplund M., Yong D., Feltzing S., Dotter A., Meléndez J., Ramírez I., 2019, arXiv e-prints, p. arXiv:1902.11008

Majewski S. R., et al., 2017, AJ, 154, 94

Marchetti T., Rossi E. M., Brown A. G. A., 2018, MNRAS, p. 2466

Marigo P., et al., 2017, ApJ, 835, 77

Martig M., et al., 2015, MNRAS, 451, 2230

Martig M., et al., 2016, MNRAS, 456, 3655

Mathur S., García R. A., Huber D., Regulo C., Stello D., Beck P. G., Houmani K., Salabert D., 2016, ApJ, 827, 50

Matsuno T., Yong D., Aoki W., Ishigaki M. N., 2018, ApJ, 860, 49

Matteucci F., Brocato E., 1990, ApJ, 365, 539

McWilliam A., 1997, ARA&A, 35, 503

McWilliam A., 2016, PASA, 33, e040

Meléndez J., et al., 2014, ApJ, 791, 14

Miglio A., et al., 2013, in European Physical Journal Web of Conferences. p. 03004 (arXiv:1301.1515), doi:10.1051/epjconf/20134303004

Mihalas D., 1970, Stellar atmospheres

Mosser B., et al., 2013, A&A, 550, A126

Murphy S. J., Shibahashi H., Kurtz D. W., 2013, MNRAS, 430, 2986

Nissen P. E., 2015, A&A, 579, A52

Nissen P. E., 2016, A&A, 593, A65

Nissen P. E., Gustafsson B., 2018, A&A Rev., 26, 6

Noguchi K., et al., 2002, PASJ, 54, 855

O'Donnell J. E., 1994, ApJ, 422, 158

Osorio Y., Barklem P. S., Lind K., Belyaev A. K., Spielfiedel A., Guitou M., Feautrier N., 2015, A&A, 579, A53

Pinsonneault M. H., et al., 2014, ApJS, 215, 19

Puls A. A., 2018, Master's thesis, Universidade Federal do Rio Grande do Sul, Porto Alegre, https://lume.ufrgs.br/handle/10183/187891

Puls A. A., Alves-Brito A., Campos F., Dias B., Barbuy B., 2018, MNRAS, 476, 690

Queiroz A. B. A., et al., 2018, MNRAS, 476, 2556

Rebassa-Mansergas A., et al., 2016, MNRAS, 463, 1137

Rodrigues T. S., et al., 2017, MNRAS, 467, 1433

Samadi R., Goupil M. J., 2001, A&A, 370, 136

Serenelli A., et al., 2017, ApJS, 233, 23

Silva Aguirre V., et al., 2018, MNRAS, 475, 5487

Simmerer J., Sneden C., Cowan J. J., Collier J., Woolf V. M., Lawler J. E., 2004, ApJ, 617, 1091

Slumstrup D., Grundahl F., Brogaard K., Thygesen A. O., Nissen P. E., Jessen-Hansen J., Van Eylen V., Pedersen M. G., 2017, A&A, 604, L8

Sneden C., Cowan J. J., Gallino R., 2008, ARA&A, 46, 241

Soderblom D. R., 2010, ARA&A, 48, 581

Spina L., Meléndez J., Karakas A. I., Ramírez I., Monroe T. R., Asplund M., Yong D., 2016, A&A, 593, A125

Spina L., Meléndez J., Casey A. R., Karakas A. I., Tucci-Maia M., 2018, ApJ, 863, 179

Stello D., Bruntt H., Preston H., Buzasi D., 2008, ApJ, 674, L53

Stello D., et al., 2009, ApJ, 700, 1589

Stello D., et al., 2013, ApJ, 765, L41

Stello D., et al., 2015, ApJ, 809, L3

Stello D., et al., 2017, ApJ, 835, 83

Tinsley B. M., 1979, ApJ, 229, 1046

Titarenko A., Recio-Blanco A., de Laverny P., Hayden M., Guiglion G., 2019, A&A, 622, A59

Tucci Maia M., Ramírez I., Meléndez J., Bedell M., Bean J. L., Asplund M., 2016, A&A, 590, A32

Twarog B. A., 1980, ApJ, 242, 242

Valentini M., et al., 2018, arXiv e-prints,

Vogt S. S., et al., 1994, in Crawford D. L., Craine E. R., eds, Society of Photo-Optical Instrumentation Engineers (SPIE) Conference Series Vol. 2198, Proc. SPIE. p. 362, doi:10.1117/12.176725

Wolf C., et al., 2018, PASA, 35, e010

Woosley S. E., Weaver T. A., 1995, ApJS, 101, 181

Woosley S. E., Heger A., Weaver T. A., 2002, Reviews of Modern Physics, 74, 1015

Yong D., Karakas A. I., Lambert D. L., Chieffi A., Limongi M., 2008, ApJ, 689, 1031

Yong D., et al., 2016, MNRAS, 459, 487

Yu J., Huber D., Bedding T. R., Stello D., Murphy S. J., Xiang M., Bi S., Li T., 2016, MNRAS, 463, 1297

Yu J., Huber D., Bedding T. R., Stello D., Hon M., Murphy S. J., Khanna S., 2018, ApJS, 236, 42